Meccanica **33:** 489–501, 1998.

Genesis of Longitudinal Vortices in Near-Wall Turbulence

W. SCHOPPA and F. HUSSAIN
University of Houston, Department of Mechanical Engineering, Houston, TX 77204-4792, U.S.A.

(Received: 26 May 1998)

Abstract. Using direct numerical simulations of turbulent channel flow, we present new insight into the formation mechanism of near-wall longitudinal vortices. Instability of lifted, vortex-free low-speed streaks is shown to generate, upon nonlinear saturation, new streamwise vortices, which dominate near-wall turbulence production, drag, and heat transfer. The instability requires sufficiently strong streaks (the wall-normal circulation on either side of a streak exceeding 7.6) and is inviscid in nature, despite the proximity of the no-slip wall. Streamwise vortex formation (collapse) is dominated by stretching, rather than Kelvin–Helmholtz rollup, of instability-generated ω_x sheets. In turn, direct stretching results from the positive $\partial u/\partial x$ (i.e. positive VISA) associated with streak waviness in the (x, z) plane, generated upon finite-amplitude evolution of the sinuous instability mode. Significantly, the three-dimensional features of the (instantaneous) instability-generated vortices agree well with the coherent structures educed (i.e. ensemble averaged) from fully turbulent flow, suggesting the prevalence of this instability mechanism. These results suggest promising new drag reduction strategies, involving large-scale (hence more durable) control of near-wall flow and requiring no wall sensors or feedback logic.

Sommario. Utilizzando una simulazione numerica diretta di flusso turbolento in un canale vengono presentate nuove prospettive sui meccanismi di formazione di vortici longitudinali vicino alla parete. Si dimostra come l'instabilità delle bande a bassa velocità e senza vortici generi, fino alla saturazione non lineare, nuovi vortici paralleli al flusso, che dominano la produzione di vorticità a parete, la resistenza e lo scambio termico. L'instabilità richiede la presenza di bande sufficientemente forti ed ha natura non viscosa, nonostante la prossimità della parete. La formazione di vortici paralleli al flusso (collasso) è dominata dallo stiramento, piuttosto che da un avvolgimento di Kelvin–Helmholtz, dei 'fogli' di ω_x generati dall' instabilità. A sua volta, lo stiramento deriva da valori positivi di ∂_u/∂_x (cioè VISA positivi) associati con le onde a bande nel piano (x, z) generate dall' evoluzione in ampiezza finita dei modi di instabilità sinusoidali. E' significativo che le caratteristiche (istantanee) three-dimensional dei vortici generati dall' instabilità concordino bene con le strutture coerenti edotte (cioè ottenute da medie d'insieme) dal flusso pienamente turbolento, il che suggerisce una prevalenza di questo meccanismo d'instabilità. Questi risultati suggeriscono nuove, promettenti strategie per la riduzione della resistenza, che utilizzino controlli di larga scala (quindi su tempi più lunghi) del flusso a parete e che non necessitino di sensori di parete o di logiche di ritorno.

Key words: Wall turbulence, Coherent structures, Vortices, Fluid mechanics.

1. Introduction

The boundary layers on transport vehicles and in industrial devices are invariably turbulent, with drastically increased drag and heat transfer at solid surfaces due to near-wall vortical coherent structures (CS). Viable control of near-wall turbulence, as yet largely unrealized in practice, has the potential to save billions of dollars per year in energy costs for engineering applications. Although massive efforts have been directed at developing drag reduction strategies, their engineering application has remained notably scarce, particularly for aircraft. The lack of success of boundary layer control to date without doubt reflects a currently limited understanding of CS initiation and evolution. In this paper, we develop a new mechanism of CS formation, well-supported by comparisons with near-wall turbulence, and briefly discuss viable large-scale control techniques.

The prominence of longitudinal vortices in near-wall turbulence is now well accepted (e.g., see [1–4]), as is their critical role in elevating drag [5] and heat transfer. The transport enhancing effect of near-wall vortices is easily understood. Due to their streamwise orientation, these vortices sweep near-wall fluid toward the wall on one flank and eject it away from the wall on the other. Drag and heat transfer are enhanced by the wallward motion, which steepens the wall gradients of streamwise velocity U and temperature, respectively. Note that the gradient reduction on the outward motion side of vortices is relatively smaller, resulting in mean transport enhancement.

Our ensemble-averaged streamwise vortices, i.e. CS [6, 7], display all previously classified near-wall features [8]. Thus, the evolutionary dynamics of streamwise CS are the essence of near-wall turbulence. The central question addressed here is: how are streamwise vortices generated? Several widely disparate formation mechanisms have been proposed, many quite plausible and self-consistent, yet currently lacking convincing validation. Thus, a formidable challenge is to identify the correct naturally and frequently occurring dynamics.

Vortex formation must recur for turbulence to be sustained; that is, existing vortices must ensure subsequent vortex regeneration. Of the numerous proposed regeneration mechanisms, most involve either: (i) the direct action (induction) of existing vortices nearby ('parent-offspring' scenarios), or (ii) local instability of a quasi-steady base flow, without directly requiring existing vortices. Note that recurring instability (ii) requires a feedback mechanism, by which previous vortices generate an unstable base flow and thus play only an indirect role.

A widely cited parent-offspring mechanism involves the generation of new vortices near existing hairpins, behind the (spanwise) arch and beside each of the (streamwise) legs (see [9] for a review). In contrast to hairpin generation, Brooke and Hanratty [10] propose that an opposite-signed offspring vortex forms immediately underneath a parent vortex, whose downstream end has lifted from the wall. Vortex formation is also often attributed to two-dimensional Kelvin–Helmholtz-type rollup of near-wall ω_x sheets (e.g. [11]), with opposite sign of the streamwise vortex existing overhead, generated by the no-slip conditin.

Of the numerous instability mechanisms developed to explain near-wall vortex formation, there is considerable disagreement as to the mechanisms of instability and feedback. For example, centrifugal [12] and Craik–Leibovich [13] instabilities, direct resonance of oblique modes [14], and local shear layer-type instabilities [15, 16] have all been proposed. Unfortunately, physical-space, vortex-dynamics representations of these mechanisms, including comparisons with near-wall turbulence, are still not at hand.

Here we demonstrate (via direct numerical simulations, DNS) that instability of streaks – without any initial (parent) vortex – directly generates new streamwise vortices, internal shear layers, and arch vortices. The instability-generated streamwise vortices are found to correspond closely with the ensemble-averaged CS educed from near-wall turbulence [7], suggesting the dominance of our proposed mechanism. Physical-space, vortex dynamics-based explanations for the vortex regeneration observed here are also provided. In the following, we outline our computational approach and important background information (Sections 2 and 3), and then demonstrate an underlying linear instability of lifted low-speed streaks (Section 4). The genesis of new vortices is illustrated in Section 5, including a brief description of the vortex dynamics involved, followed by the associated regeneration mechanism and implications for boundary layer control (Section 6). Additional details of these results may be found in [17].

2. Computational Approach

In the following, we address vortex regeneration using direct numerical simulations of the Navier – Stokes equations. Periodic boundary conditions are used in x and z, and the no-slip condition is applied on the two walls normal to y; see [18] for the simulation algorithm details. The spatial discretization and Re are chosen so that all dynamically significant lengthscales are resolved (i.e. a finer computational grid does not markedly affect the solution); thus, no subgrid-scale turbulence model is necessary. Code validation and accuracy checks were performed by comparing the growth rates for simulated two-dimensional and three-dimensional Orr–Sommerfeld modes of the laminar (parabolic profile) flow with independent stability analysis (agreement within 1%).

To better isolate instability and the subsequent vortex formation, we use the minimum outer Reynolds number $\text{Re} = U_c h/\nu = 2000$ (U_c is the centerline velocity of the $2h$ wide channel) and the minimum domain sizes in x and z for sustained channel flow turbulence – the so-called 'minimal flow unit' of [19]. For the simulations of isolated vortex regeneration, a constant volume flux is maintained, and $32 \times 129 \times 32$ grid points are used in x, y, and z, respectively.

3. Background

3.1. Vortex Definition

The mere identification of near-wall vortices, typically embedded within the background ω_z, has proven to be a major challenge in itself. Popular free shear flow vortex identification techniques, such as $|\omega|$ isosurfaces or vortex line bundles, are generally ineffective near the wall (where $|\omega|$ is very large even outside CS, primarily due to ω_z). As alternatives, low pressure, ω_x, and closed streamlines in (y, z) planes have all been used to identify streamwise vortices in DNS data.

The limitations of these existing definitions have been analyzed by Jeong and Hussain [20], who then went on to develop a general-purpose vortex definition, which isolates local pressure minima induced solely by vortices. That is, *vortices are regions of negative* λ_2, the second largest eigenvalue of the tensor $S_{ik}S_{kj} + \Omega_{ik}\Omega_{kj}$, where S_{ij} and Ω_{ij} are the symmetric and antisymmetric parts of $\partial u_i/\partial x_j$, respectively. This definition has been validated for a variety of vortical flows, including both DNS data and analytical solutions, even in situations when other definitions (e.g. [21, 22]) may not hold.

3.2. Near-Wall Coherent Structures

To establish the most frequently occurring vortex geometry (i.e. CS), we ensemble average a large number of properly aligned vortex realizations (i.e. CS education). The λ_2 definition is first used to quantify fully three-dimensional near-wall vortices (below $y^+ = 60$) in DNS data [18], for each sign of ω_x. Only fully-formed 'mature' vortices are accepted for ensemble averaging, enforced by constraints on the vortices' λ_2 magnitude ($\lambda_2 < -\lambda_{2\text{rms}}$) and minimum x extent ($\Delta x^+ = 150$). To extract the entire extent of fully three-dimensional CS, the maximum permissible deviation of the vortex axis from x is specified as 30° (appropriate for quasi-streamwise vortices). Accepted vortices of a given sign are aligned at the midplane of their x extent before ensemble averaging.

To account for their possible geometric differences, we educe two separate sets of streamwise vortices: those with positive ω_x (called SP) and negative ω_x (SN). As shown in Figure 1, the

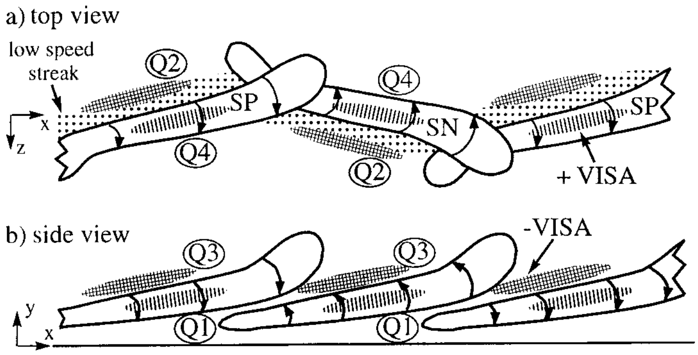

Figure 1. Near-wall educed CS and associated coherent events (adapted from [7]); including $\pm$ VISA events ($\pm\partial u/\partial x$); quadrant Re stresses Q1, Q2 (ejection), Q3, and Q4 (sweep); and a kinked low-speed streak.

educed SP and SN are symmetric counterparts, both inclined 9° to the wall and tilted from x on each side by 4° (exaggerated in Figure 1) in the top view. The relative spatial orientation of SP and SN is determined by aligning realizations at either end of accepted λ_2 events with $+\omega_x$ or $-\omega_x$. That is, eduction aligned at one end of SP automatically captures the adjacent end of SN and vice-versa. Note that vortices neighboring in z do not survive in the ensemble average, as would otherwise be the case if hairpin vortices were predominant. Although vortex line bundles exhibit obvious hairpin shapes, these should not be confused with elongated hairpin *vortices* (identified by λ_2), which do not seem to occur frequently near the wall.

From the three-dimensional u and ω fields and their ensemble averages, we have developed a conceptual model of the near-wall CS which captures well all features observed or measured previously. In Figure 1, we show the locations relative to SP and SN of identified low-speed streaks, quadrant Re stress events (Q1, Q2, Q3, Q4), and positive and negative $\partial u/\partial x$ (i.e. VISA events, the spatial counterpart of VITA $\partial u/\partial t$) events studied experimentally, which can be related by Taylor's hypothesis). These results are discussed in more detail in [6, 7].

4. Streak Instability

4.1. Minimal Channel Flow

Our own analysis of minimal channel regeneration suggests the presence of an underlying streak instability. During the quiescent phase of the regeneration cycle, when the wall shear stress is minimum, the buffer region contains only a lifted-up, long, low-speed streak, with no significant streamwise vortices or even ω_x. Shortly thereafter ($t^+ \sim 40$ later), a new positive streamwise vortex is created (by instability, as shown here) in the buffer region from the vorticity sheet (predominantly $+\omega_y$) flanking the streak. Thus, the observed large temporal variations in integrated wall shear stress directly reflect the vortex regeneration: the drag is minimum during the quiescent phase, when near-wall vortices are very weak, and maximum once collapsed streamwise vortices (which bring high-speed fluid toward the wall to increase drag) are generated in the buffer layer. These observations suggest that 'vortex-less' low-speed streaks are unstable and serve as an agent of vortex regeneration. In full-domain flows as well, extremely long ($\Delta x^+ \sim 1000$) streaks are prevalent, and many regions along individual streaks are devoid of any streamwise vortices [4].

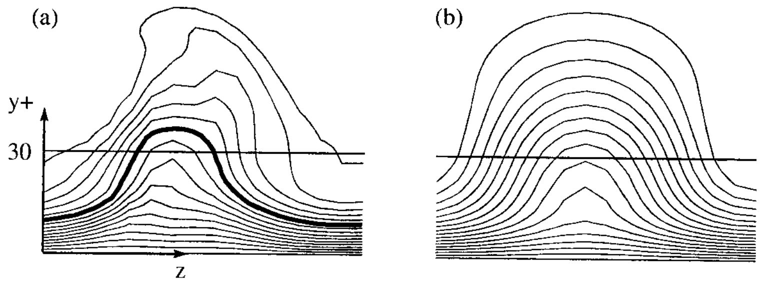

Figure 2. Low-speed streak at the quiescent phase of minimal channel regeneration, illustrated by (a) a typical cross-stream distribution of U and (b) the analytical base flow (1) used for analysis.

To isolate instability of vortex-less streaks, we consider a base flow of the form

$$\begin{aligned} U^+(y^+, z^+) &= U_0^+(y^+) + (\Delta u_0^+/2)\cos(\beta^+ z^+)(y^+/30)\exp(-\boldsymbol{\sigma} y^{+2} + 0.5), \\ V^+ &= W^+ = 0, \end{aligned} \tag{1}$$

as a first approximation, where U_0^+ is the turbulent mean velocity profile. The streak's normal circulation per unit length Δ_{u0}^+, spanwise wavenumber β^+ and transverse decay $\boldsymbol{\sigma}$ are chosen to approximate a typical U distribution, shown in Figure 2(a) for minimal channel flow. The corresponding (y, z) distribution of (1) with $\Delta_{u0}^+ = 11.2, \beta^+ = 0.06$ (i.e. streak spacing $\Delta_z^+ = 100$), and $\boldsymbol{\sigma} = 0.00055$ (i.e. maximum streak ω_y at $y^+ = 30$) is shown in Figure 2(b) and closely resembles the instantaneous realization in Figure 2(a). Note that the base flow (1) contains no ω_x and is a steady solution of the Euler equations.

4.2. Linear Stability Analysis

With the base flow (1) frozen and Re $= 2000$, we find exponential growth of linear amplitude sinuous perturbations (i.e. streak bending in *z* commonly observed), indicating that lifted streaks (1) are indeed linearly unstable. The instability growth is characterized in the following by $E_{10}(t)$, the volume-integrated energy in Fourier modes with a *z*-wavenumber of 0 (mean in *z*) and an x-wavenumber of α (x-fundamental mode). Interestingly, enhanced growth of E_{10} with increasing Re reflects an inviscid instability mechanism, found to be quite similar in nature to oblique instability modes of free shear layers. Consequently, viscous effects and the no-slip wall play no destabilizing role. This raises the question: how does viscosity, obviously crucial near the wall, enter the instability dynamics?

We find that the viscous damping of instability is quite strong for a streak spacing of $\Delta z^+ = 100$, the popularly accepted value. Since the peak E_{10} occurs at a linear amplitude (i.e. three-dimensional perturbation amplitudes near machine accuracy; see Figure 3(b), the typical nonlinear (i.e. finite-amplitude) saturation is not occurring here. Instead. attenuation is due primarily to cross-diffusion (i.e. viscous annihilation, a kind of planar reconnection) of the opposite-signed ω_y flanking the low-speed streak. In fact, ω_y is reduced to 68% of its initial value by the E_{10} saturation time, indicating that the (exponential) streak decay rate due to cross-diffusion (Figure 3(d)) is non-negligible (approximately half the instability growth rate; Figure 3(b)).

We now consider the instability scaling at higher Re, keeping $\Delta z^+ = 100$ fixed. As shown in Figures 3(b,d), both instability growth and streak diffusion (annihilation of normal circulation Δu^+) scale well in (inner) wall units. Although this is perhaps not surprising because of the

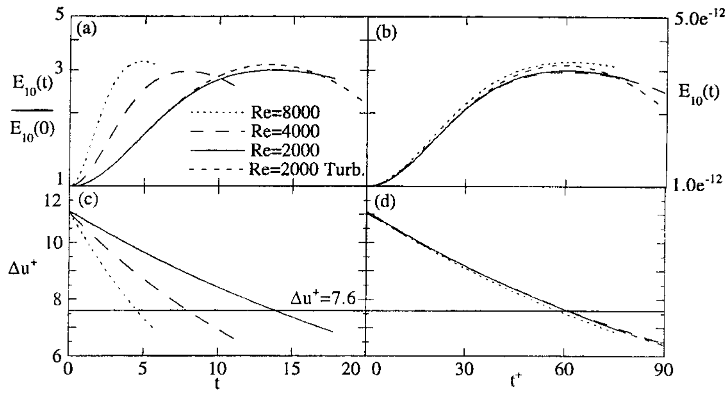

Figure 3. Temporal evolution of (a, b) E_{10} and (c, d) streak y circulation as a function of Re in (a, c) dimensional and (b, d) wall time units, for a constant streak spacing $\Delta z^+ = 100$. The data collapse in (b,d) illustrate the inner scaling and balance of streak instability and viscous streak annihilation, showing Re invariance. Except for the case with a turbulent mean profile, the Reichardt relation is used for $U_0^+(y^+)$ in (1).

absence of outer vortices in these flows, the possibility of autonomous inner-scaling dynamics clearly exists. These results demonstrate that streak instability grows similarly at higher Re (perhaps even at very high Re), provided that the streak velocity profile is self-similar in wall units. By considering the dimensional time evolution, one can see how this is possible. As Re is increased, the wall vorticity Ω_w (i.e. $U(y)$ slope) increases (according to the Blasius skin friction law), and the (dimensional) streak spacing decreases. Consequently, the streak annihilation by cross-diffusion is faster at higher Re (Figure 3(c)), but the instability growth rate is also enhanced due to concomitant increased wall vorticity (Figure 3(a)), their balance maintaining a nearly constant E_{10} amplification. Figures 3(b,d) also confirm the stabilizing role of viscous cross-diffusion across streaks; saturation occurs in each case at a critical normal circulation of $\Delta u^+ = 7.6$. Note that Δu^+, being a measure of the tilt angle of the vortex lines (in (y, z)) on either side of a streak, represents the extent of streak lifting (i.e. the crest amplitude of u contours in Figure 2). Thus, sufficient lift-up of the low-speed streak into the buffer layer is required for instability to occur. In the following, we focus on the more computationally tractable Re $= 2000$ case, noting that the streak instability is generic to higher Re.

5. Vortex Formation Mechanism

Having confirmed that (one-walled) streaks with sufficient y circulation (Δu^+) are indeed linearly unstable, we now consider the subsequent nonlinear evolution using DNS. Results clearly illustrate the genesis of streamwise CS, near-wall shear layers, and arch vortices, suggesting that streak instability is the dominant mechanism of vortex generation and thus turbulence production.

5.1. Streamwise Vortices

Most significantly, as the mode grows to a nonlinear amplitude (initially $w'/U_c = 1\%$ at $y^+ = 30$), new collapsed streamwise vortices are directly created (Figure 4(a-c)). At early times, instability growth is characterized by increased circulation of flattened ω_x sheets, with the spanwise symmetry of the linear eigenmode approximately maintained. Subsequently, as nonlinear effects (described below) become prominent, $+\omega_x$ begins to concentrate on the $+z$

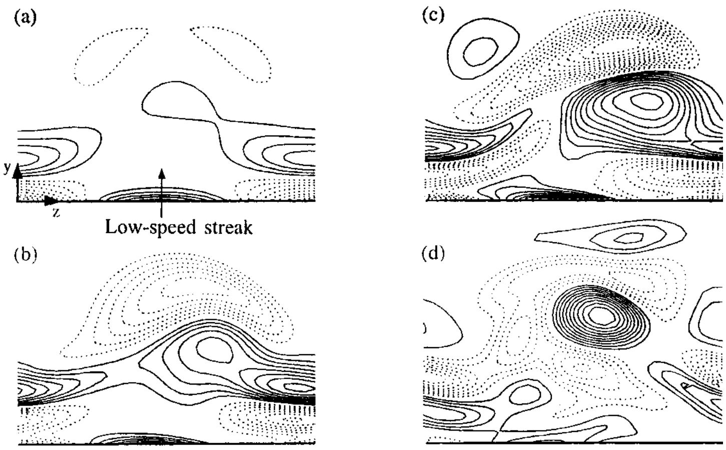

Figure 4. Streamwise vortex formation due to finite-amplitude streak instability, illustrated by cross-stream distributions of ω_x at (a) $t^+ = 17$, (b) $t^+ = 51$, (c) $t^+ = 103$, (d) $t^+ = 928$. Planes in (b) and (c) are tracked with the instability phase speed of approximately $0.6\,U_c$.

flank of the low-speed streak (Figure 4(b)). By symmetry, the ω_x distribution at a half wavelength in x away is obtained by z reflection and sign inversion; thus, $-\omega_x$ is generated on the $-z$ flank here. As this ω_x amplification continues, collapsed (i.e. with compact cross-section) streamwise vortices quickly emerge (Figure 4(c)). This genesis of new vortices from ω_x layers is strikingly similar to that frequently observed in minimal channel flow. Previous studies (e.g. [11]) presumed that the layer simply rolls up due to its own (two-dimensional) advection. Our results (discussed below) indicate that the vortex formation is not in reality a (Kelvin–Helmholtz type) roll up process; the formation is inherently three-dimensional, dominated by intense ω_x stretching. Even well past their initial formation, streamwise vortices and hence turbulence continue to be sustained (e.g. Figure 4(d)), indicating the importance of streak instability to turbulence sustenance.

The three-dimensional geometry of the instability-generated vortices (Figures 5(a,b)) (say, the x-overlapping of tilted, opposite-signed streamwise vortices on either side of a low-speed streak) agrees well with the typical flow structure during the active phase of minimal channel regeneration. Most significantly, this vortex geometry (maintained upon evolution except for increasing overlap) is strikingly similar to that of three-dimensional CS educed (from more than 100 vortex realizations) in full-domain turbulence (Figure 1), which has been shown to capture all important near-wall events [7]. Irregularities (e.g. kinks) of the base flow streaks and finite-amplitude incoherent turbulence will surely occur, causing variations in vortices from one realization to another. If an underlying instability mechanism is present, it should be revealed by ensemble averaging over a large number of base flow/perturbation combinations, that is, by CS eduction. The close correspondence of Figures 1 and 5 indicate that this is in fact the case, serving as strong evidence that this vortex formation process is a dominant mechanism in fully developed near-wall turbulence.

Since the newly generated vortices are predominantly streamwise (Figure 5(a)), the essential dynamics of vortex formation are those of ω_x, whose inviscid evolution is governed by

$$\frac{\partial \omega_x}{\partial t} = -u\frac{\partial \omega_x}{\partial x} \underbrace{- v\frac{\partial \omega_x}{\partial y} - w\frac{\partial \omega_x}{\partial z}}_{\text{Self-induction}} + \underbrace{\omega_x\frac{\partial u}{\partial x}}_{\text{Stretching}} + \underbrace{\frac{\partial v}{\partial x}\frac{\partial u}{\partial z} - \frac{\partial w}{\partial x}\frac{\partial u}{\partial y}}_{\text{Tilting}}. \tag{2}$$

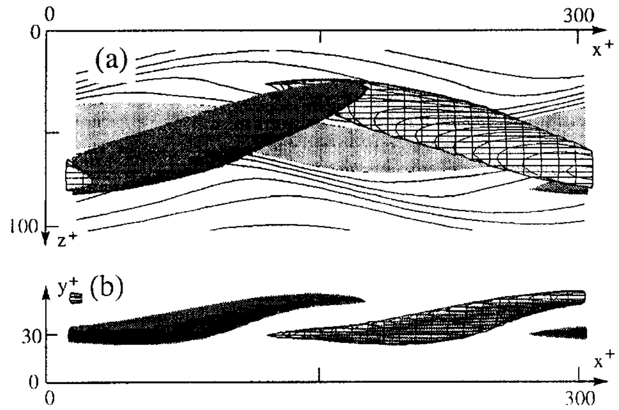

Figure 5. Streamwise vortices' (x, z) plane tilting, x-overlapping, and location relative to a low-speed streak in (a) top view, (b) side view. The 80% isosurfaces of $+\omega_x$ and $-\omega_x$ at $t^+ = 103$ are (dark) shaded and hatched respectively; contours of u at $y^+ = 20$ are overlaid in (a), with low levels of u light-shaded to demarcate the low-speed streak. Note the striking resemblance of this instantaneous realization with the ensemble-averaged CS (Figure 1).

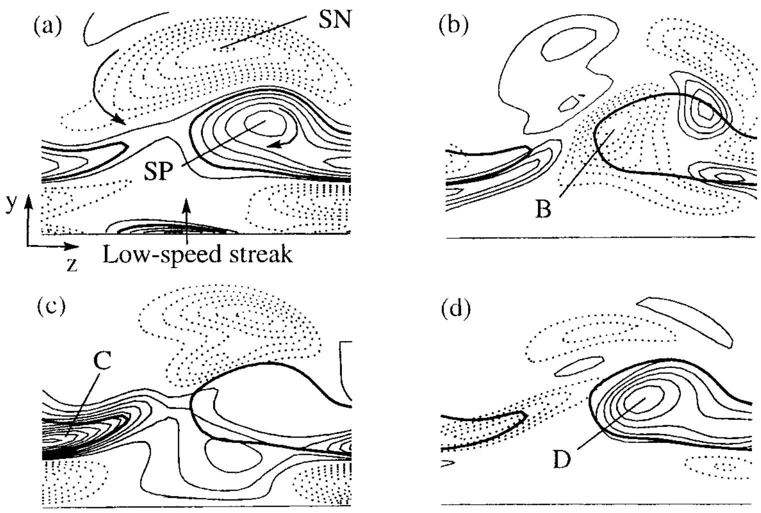

Figure 6. Distributions of (a) ω_x, and selected terms of the ω_x evolution equation: (b) self-induction (cross-stream), (c) the $-(\partial w/\partial x)$ $(\partial u/\partial y)$ tilting term, and (d) direct stretching $(\omega_x \partial u/\partial x)$; (a–d) are at an intermediate time during vortex formation ($t^+ = 51$). The bold line in each panel identifies the ω_x layer.

In Figure 6, we observe that the circulation of the elongated near-wall ω_x layers (Figure 6(a)) increases due to vortex line tilting, given by the latter production term $-(\partial w/\partial x)(\partial u/\partial y)$ (Figure 6(c)), which dominates the former. Although typically largest in magnitude over all other, the $-(\partial w/\partial x)$ $(\partial u/\partial y)$ term actually generates a flattened tail in the near-wall ω_x layer (C in Figure 6(c)), not a vortex. Contrary to prior speculation, these layers do not roll up due to their self-advection – a purely two-dimensional mechanism. In fact, the cross-stream transport (B in Figure 6(b)) actually opposes the rollup process, due to the opposite-signed ω_x immediately overhead (SN in Figure 6(a)). In reality, vortex formation is due to direct stretching of $+\omega_x$ on the $+z$ flank of the low-speed streak (also, $-\omega_x$ amplification on the $-z$ flank, at a half x wavelength away), evident from nearly circular regions of $+\omega_x \partial u/\partial x$ there (D in Figure 6(d)). We find that this local ω_x stretching is sustained in time and is mainly responsible for the eventual vortex collapse, whose location coincides with the $+\omega_x \partial u/\partial x$ peak (cf. Figures 4(c) and 6(d)).

In turn, the positive $\partial u/\partial x$ responsible for vortex collapse by stretching is a simple consequence of low-speed streak waviness, illustrated in Figure 5(a). Recall that streak waviness is generated by (linear) sinuous streak instability. Once this waviness grows to a finite size, strong $+\partial u/\partial x$ develops downstream of the streak crests, causing direct stretching of positive (SP) and negative (SN) ω_x existing there. Since a large velocity difference exists across the streak flanks (with vorticity comparable to the mean velocity gradient at the wall), a sizable value of $+\partial u/\partial x$ is quickly generated by the rapidly growing (initially exponentially) streak wave. The initial ω_x sheets (Figure 4(a)) then suddenly collapse (Figure 4(c)) due to localized stretching (Figure 6(d)), overcoming viscous diffusion which would otherwise cause their annihilation (on a similar timescale as the collapse). Note that these dynamics are also captured as (ensemble-averaged) +VISA events (i.e. $+\partial u/\partial x$) existing within the CS core (Figure 1), indicating that this vortex generation process is indeed a dominant one.

5.2. Internal Shear Layers and Arch Vortices

The significance of (nonlinear) streak instability is not limited to streamwise vorte formation; it also captures the genesis of new internal shear layers and spanwise arch vortices. Internal shear layers, indicated by wall-detached sheets of ω_z, form alongside (in z) the generated streamwise vortices (Figures 7(a,b)). Subsequently, the downstream 'end' of the internal shear layer rolls up into a new (locally spanwise) arch vortex (Figures 7(d,f)). A surprising result is that the downstream tips of (newly generated) streamwise vortices tilt and propagate outward to form

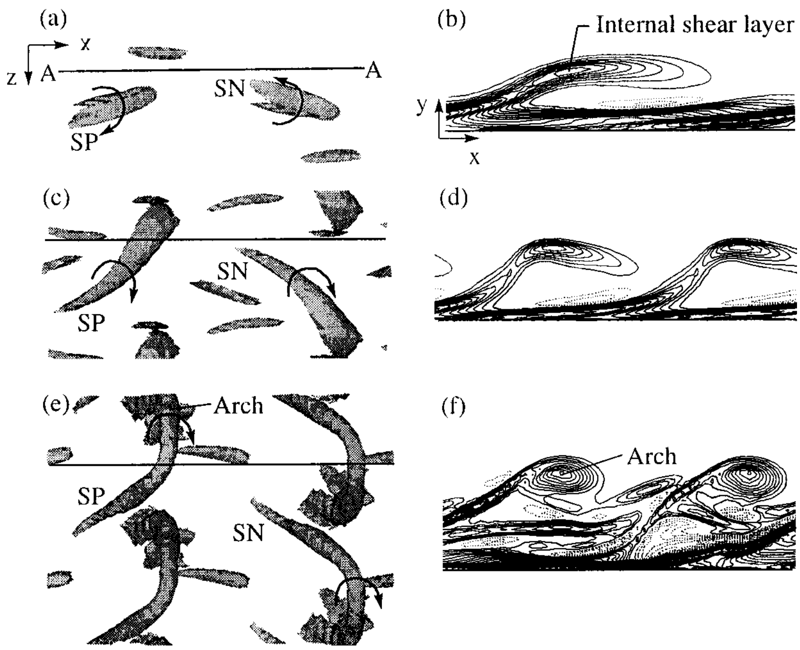

Figure 7. Genesis of internal shear layers and arch vortices due to nonlinear evolution of streak instability, illustrated by actual DNS data. (a,c,e): the evolutions of vortices SP and SN (top view) represented by λ_2 isosurfaces; (b,d,f): corresponding contours of ω_z in the section A-A (the straight line in a,c,e) indicating internal shear layer and arch vortex formation.

arches (Figures 7(c,e)). Note that this process, i.e. streak instability→streamwise vortices→arch vortices, is contrary to the mechanism proposed in [4], i.e. streak instability → archvortices → streamwise vortices. Direct formation of arches through instability is unlikely, since the corresponding instability would involve varicose modes, found to be *stable* for relevant streak distributions [17]. In minimal channel flow, we find that arches without legs are commonly created, not by instability, but by viscous annihilation of a leg originally attached to an arch (like the vortices in Figure 7(e)).

6. Regeneration Mechanism and Control

We now consider scenarios by which streak → vortex → streak (or equivalently vortex → streak → vortex) regeneration might occur. Each case relies on the same underlying regeneration mechanism, i.e. vortex formation due to streak instability and streak formation by vortices, established rather rigorously here. Thus, a dominant underlying mechanism occurs although each vortex formation process superficially appears to be different.

As argued earlier, the long lifted low-speed streaks observed, coupled with the rapid streak diffusion, indicates that a given streak is sustained by strings of streamwise vortices advecting (faster) overhead. In turn, we have demonstrated that the important near-wall structures (streamwise vortices, internal shear layers, arch vortices) are generated from initially vortex-less low-speed streaks by instability. This suggests that vortex-less streaks are necessary *nucleation sites* for vortex regeneration.

The scenarios outlined in Figure 8 indicate possible ways in which vortex-less streaks (susceptible to instability and vortex formation) can arise. For process A in Figure 8, regeneration occurs in a naturally occurring 'gap' between x-neighboring vortices along the streak. Such gaps are common in reality [4], indicating natural irregularities in the vortex regeneration occurring upstream. Alternatively, streaks can appear with arches overhead (process B), but without streamwise vortices (due to viscous annihilation of streamwise vortices by crowding, observed by us in minimal channel flow). In this case, the *w(x)* induced by the tilted arch excites (finite amplitude) streak instability, generating a leg (q in Figure 8) propagating (upstream)

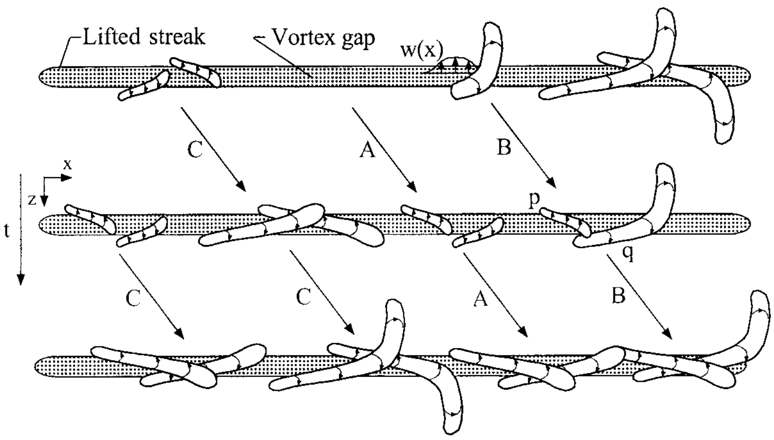

Figure 8. Spatiotemporal scenarios for vortex regeneration by instability of vortex-less streaks. Process A: regeneration within gaps between (existing) neighboring vortices. Process B: regeneration from an existing arch vortex, whose $w(x)$ profile shown excites streak instability to produce a pair of new streamwise vortices. Process C: regeneration at trailing ends of low-speed streaks.

from the arch and also a new opposite-signed streamwise vortex (p in Figure 8). Intuitively, we expect that the trailing ends of lifted low-speed streaks will be prominent nucleation sites for regeneration, as illustrated by process C. Due to the faster advection of vortices relative to streaks, these streak ends are 'self-cleaning' in that the new vortices spawned are advected downstream. Due to their induction, the vortices sustain the streak near its trailing end, eventually leaving behind a lifted vortex-less streak (as behind the vortex pair in Figure 8). Subsequently, incoming (incoherent) perturbations pass over the streak end, exciting streak instability and spawning a new set of streamwise vortices, and so on.

The association of vortex formation with an instability is promising from a control standpoint, noting the success of instability control in free shear flows. The most logical approach to CS-based drag reduction and heat transfer suppression is to simply prevent vortex regeneration in the first place (in contrast to the MEMS approach to counteract fully developed CS). To suppress CS via control of streak instability, there are two possibilities: either (i) counteract existing perturbations which would otherwise excite instability, or (ii) stabilize (at least partially) the base flow streaks. Pursuit of (i) would necessitate small-scale control (~ 0.1 mm for engineering applications), which would suffer from the durability problems of MEMS. Approach (ii) is very attractive from the standpoint of large-scale control, wherein numerous (perhaps hundreds) streaks may be simultaneously stabilized by a single large-scale forcing.

To test these ideas, we are currently considering new large-scale control techniques aimed at streak stabilization [23]. In particular, we are investigating drag reduction by (i) a spanwise row of counter-rotating, x-independent streamwise vortices, centered in the outer region (at the channel centerline), and (ii) colliding spanwise wall jets. It is important to note that we focus on large-scale control, in which the flow forcing has a spanwise wavelength much larger than the characteristic streak spacing. Due to an attenuation of streak strength (i.e. y-circulation) by viscous cross-diffusion, and hence, suppression of new CS formation, we find that a significant drag reduction is attained. Note that our technique involves no wall or flow oscillations and a very low forcing amplitude, in contrast to the high frequency oscillation effect (infeasible to implement at practical Re) reported, but not explained, in [24]. Our control approach is particularly attractive from a practical standpoint, in which no sensors are required (necessary for adaptive feedback control) and large-scale (hence more durable and feasible) actuation is effective. The forcing is passive and time-independent. Further details of our large-scale control strategies are beyond the scope of this paper (see [23]).

7. Concluding Remarks

To summarize, we have shown that (nonlinear) instability of ejected low-speed streaks, initially without any vortices whatsoever, directly generates new streamwise vortices, internal shear layers, and arch vortices. The resulting three-dimensional vortex geometry is identical to that of the dominant CS, educed from fully developed near-wall turbulence, which, in turn, capture all important, extensively reported near-wall events. This serves as strong evidence that vortex-less streaks are the main breeding ground for new streamwise vortices, commonly accepted as dominant in turbulence production. In turn, the geometry of the newly generated vortices constitutes a built-in mechanism which sustains ejected streaks against their otherwise rapid self-annihilation due to cross-diffusion. Vortex-less streaks, the vehicle for instability-based vortex formation, are expected to arise inherently due to the differential advection of vortices and the streaks they generate.

Since vortex formation and turbulence production are critically reliant on lifted low-speed streaks, large-scale (relative to the natural streak spacing) control of streaks is a potentially effective approach to drag reduction, noting the tiny scale of near-wall structures in most engineering situations. We have found that large-scale drag reduction is in fact effective via either counterrotating vortex generators or colliding spanwise wall jets. Our control approach is particularly attractive from a practical standpoint, in which no sensors are required (necessary for adaptive feedback control) and large-scale (hence more durable and feasible)actuation is effective.

Acknowledgements

This research was supported by AFOSR grant F49620-97-1-0131 and the NASA Graduate Fellowship grant NGT-51022 of W.S.

References

1. Townsend, A.A., *The Structure of Turbulent Shear Flows*, Cambridge, 1956.
2. Kline, S.J., Reynolds, W.C., Schraub, F.A. and Rundstadler, P.W., 'The structure of turbulent boundary layers', *J. Fluid Mech.* **30** (1967) 741.
3. Blackwelder, R.F. and Eckelmann, H., 'Streamwise vortices associated with the bursting phenomenon', *J. Fluid Mech.* **94** (1979) 577.
4. Robinson, S.K., 'Coherent motions in the turbulent boundary layer', *Ann. Rev. Fluid Mech.* **23** (1991) 601.
5. Kravchenko, A.G., Choi, H. and Moin, P., 'On the relation of near-wall streamwise vortices to wall skin friction in turbulent boundary layers', *Phys. Fluid A* **5** (1993) 3307.
6. Jeong, J. and Hussain, F., 'Coherent structures near the wall in a turbulent channel flow', In: K.S. Chang and H. Choi (eds), *Proc. Fifth Asian Congress of Fluid Mech.*, Taejon, Korea, 1992, pp. 1262.
7. Jeong, J., Hussain, F., Schoppa, W. and Kim, J., 'Coherent structures near the wall in a turbulent channel flow', *J. Fluid Mech.* **332** (1997) 185.
8. Kline, S.J. and Robinson, S.K., 'Quasi-coherent structures in the turbulent boundary layer: Part 1. Status report on a community-wide survey of the data', In: S.J. Kline and N.H. Afgan (eds), *Near-Wall Turbulence* Hemisphere, 1990.
9. Smith, C.R. and Walker, J.D.A. 'Turbulent wall-layer vortices', In: S. Green (ed.), *Fluid Vortices*, Springer, 1994.
10. Brooke, J.W. and Hanratty, T.J., 'Origin of turbulence-producing eddies in a channel flow', *Phys. Fluids A* **5** (1993) 1011.
11. Jimenez, J. and Orlandi, P., 'The rollup of a vortex layer near a wall', *J. Fluid Mech.* **248** (1993) 297.
12. Brown, G.L. and Thomas, A.S.W., 'Large structure in a turbulent boundary layer', *Phys. Fluids* **20** (1977) 5243.
13. Phillips, W.R.C. and Wu, Z., 'On the instability of wave-catalysed longitudinal vortices in strong shear', *J. Fluid Mech.* **272** (1994) 235.
14. Jang, P.S., Benney, D.J. and Gran, R.L., 'On the origin of streamwise vortices in a turbulent boundary layer', *J. Fluid Mech.* **169** (1986) 109.
15. Swearingen, J.D. and Blackwelder, R.F., 'The growth and breakdown of streamwise vortices in the presence of a wall', *J. Fluid Mech.* **182** (1987) 225.
16. Hamilton, J., Kim, J. and Waleffe, F., 'Regeneration mechanisms of near-wall turbulence structures', *J. Fluid Mech.* **287** (1995) 317.
17. Schoppa, W. and Hussain, F., 'Genesis and dynamics of coherent structures in near-wall turbulence', In: R. Pantons (ed.), *Self-sustaining Mechanisms of Wall Turbulence*, Computational Mechanics Publications, 1997a, pp. 385.
18. Kim, J., Moin, P. and Moser, R.D. 'Turbulence statistics in fully developed channel flow at low Reynolds number', *J. Fluid Mech.* **177** (1987) 133.
19. Jimenez, J. and Moin, P., 'The minimal flow unit in near-wall turbulence', *J. Fluid Mech.* **225** (1991) 213.

20. Jeong, J. and Hussain, F., 'On the identification of a vortex', *J. Fluid Mech.* **285** (1995) 69.
21. Hunt, J.C.R., Wray, A.A. and Moin, P., 'Eddies, Stream, and Convergence Zones in Turbulent Flows', Center for Turbulence Research Rep., CTR-**S88**, 1988, p. 193.
22. Chong, M.S., Perry, A.E. and Cantwell, B.J., 'A general classification of three- dimensional flow field', *Phys. Fluids A* **2** (1990) 765.
23. Schoppa, W. and Hussain, F., 'Effective drag reduction by large-scale manipulation of streamwise vortices in near-wall turbulence', Presented at: *4th AIAA Shear Flow Control Conference*, Snowmass CO, AIAA Paper No. AIAA **97**–1794.
24. Jung, W.J., Mangiavacchi and Akhavan, R., 'Suppression of turbulence in wall-bounded flows by high-frequency spanwise oscillations', *Phys. Fluids A* **4** (1992) 1605.